Structure and Growth of Tumors: The Effect of Cartesian, Cylindrical, and Spherical Geometries

RIZWAN-UDDIN[a,b] AND IBRAHIM M. SAEED[c]

[a] *Department of Nuclear Engineering, (also, Computational Science and Engineering Program) University of Illinois at Urbana-Champaign, Urbana, Illinois 61801, USA*
[c] *School of Medicine, Medical College of Virginia, Virginia Commonwealth University, Richmond, Virginia 22903, USA*

ABSTRACT: We present results of numerical simulations of a mathematical model simulating mass transfer in the development of a tumor, resulting in its encapsulation and lobulation. A modified generation term that reflects the population pressure on growth leads to nodular tumor growth. Simulations have been carried out in one dimensional Cartesian, cylindrical, and spherical geometries. Important differences between the three cases have been found. Simulation results in spherical geometry suggest the lobes near the center of the tumor to be larger than those near the capsule wall.

INTRODUCTION

A good understanding of tumor evolution is essential for the development of an efficient prevention and cure. Tumors, whether benign or malignant, are composed of two basic components: (1) cancerous cells that constitute its parenchyma, and (2) supportive stroma made of connective tissue and blood vessels. Since tumors have the potential to arise from any cell or body tissue, there are a wide variety of structural appearances seen, contributing to the difficulty in classifying a tumor as either benign or malignant. The distinction between benign and malignant tumors is based on many criteria: degree of differentiation, rate of growth, local invasion, and metastatic ability. Benign tumors are usually well-differentiated, slow growing and cannot metastasize; whereas malignant tumors are usually poorly differentiated, fast growing, and can metastasize. Next to metastases, invasiveness is the most reliable feature that differentiates a benign tumor from a malignant one.

[b]Address for correspondence: Department of Nuclear Engineering, University of Illinois at Urbana-Champaign, 103 South Goodwin Avenue, Urbana, Illinois 61801, USA. Phone, 217/244-4944; fax, 217/333-2906; e-mail, rizwan@uiuc.edu

Benign tumors are often contained in a dense band (or capsule) comprised of connective tissue. Encapsulated benign tumors are either a continuum of tumor cells, or appear as several lobes of different sizes (*multinodular*), separated by a small amount of intervening connective tissue stroma, all contained in a larger capsule. A good understanding of the growth and encapsulation process in benign tumors may lead to the development of artificial means of inducing it, and hence containing the spread of malignant tumor cells.[1,2]

There are currently three hypotheses that attempt to explain the encapsulation process: the Expansive Growth Hypothesis (EGH); the Foreign Body Hypothesis (FBH); and the Wound-Healing Hypothesis (WHH).[3,4] According to the EGH, the connective tissue matrix adjacent to the initial site of tumorous mutation is simply "pushed" outward in a ring, by the multiplying tumorous cells, leading to a thin region of highly concentrated connective tissue, which then *gels* (*pressure atrophy*) into a circumferential capsule, composed of an extracellular collagenous matrix. This hypothesis suggests that the fibrous capsule is formed passively from condensed, mature pre-existing collagen. Although this may be true of some tumors, subsequent observations by Barr *et al.*[4] using thymidine autoradiography shows a proliferation of endothelium within capsules at a rate similar to that of the tumor endothelium itself, indicating that for some tumors at least, there is an active process of collagen deposition that may also take place.

Under the FBH, the human body, on learning the presence of the tumorous cells, treats the tumor as a foreign and undesirable intruder, and creates a barrier (the capsule) to contain the tumor.[5,6,7] Though there is some evidence supporting FBH,[8] other evidence suggests that this hypothesis is unlikely.[4,9] Moreover, the process by which the capsule is formed is not entirely clear. The major distinction between the EGH and the FBH is that the latter is an active process, while the former is a passive phenomenon.

The third hypothesis (WHH) has some features similar to the other two hypotheses, and it resolves some of the discrepancies that EGH and FBH have with observed tumor characteristics. According to WHH, tumor stroma is generated in a process similar to the three-step wound healing mechanism—extravasation of proteins, formation of granulation tissue, and transition to collagen.[3,4,10] Hence, the first step in stroma generation is the extravasation of proteins commonly found in plasma, including plasminogen, fibronectin, and fibrinogen. The last of these clots, is cleaved, and cross-linked to fibronectin, becoming a gel that is both insoluble and can retain water. This gel of extravascular fibrin-fibronectin serves as both a matrix for immigrating macrophages, fibroblasts, and new capillaries, and is degraded and transformed into granulation tissue, which itself eventually becomes relatively dense and acellular collagen. This hypothesis suggests a transition of connective tissue into a fibrous capsule. The theorized difference between wound healing and tumor generation is that while the former process is self-limiting, the latter persists and new gel can be continuously deposited. While the classic wound gets healed over a short period of time, an encapsulated tumor persists.

Mathematical modeling of tumor growth has, in general, been restricted to simple models.[11-13] Evaluation of tumor growth models was reported by Vaidya and Alexandro[14]. Recent developments in the understanding of the convection-diffusion and reaction-diffusion equations,[15,16] their application to mathematical biology,[17-19] and progress in numerical schemes to solve these equations,[20] has led to modeling of tumor growth as a reaction-diffusion process.[2,10,21,22] It is also becoming possible to infer the physical mechanism of unexplained phenomena—such as nodular tumors—by comparing the

simulation results of models based on hypothesized phenomena with clinical observations and laboratory data.

Perumpanani *et al.*[22] developed and numerically solved two mathematical models in one-dimensional Cartesian geometry to explain the formation of the capsule and the multi-nodular nature of some tumors. Their first mathematical model consists of two partial differential equations (PDEs), and the more detailed second model consists of four PDEs. The differential equations in the simpler model represent the balance of tumor cells (TC) and connective tissue (CT). The two additional equations in the more detailed model represent protease and normal cell concentrations. Their model predicts a thin dense layer (high concentration) of CT that encloses the tumor cells. This dense layer—that in a concentration profile looks like a wall—eventually *gels* and forms the capsule. Lobular structure, according to their model, results from the small concentration of the tumorous cells that manage to diffuse ahead of the accumulating concentration of CT at the *wall*. The tumor cells that manage to escape outside the first wall of CT then multiply, push the existing CT beyond the *wall* further outward, and lead to a second wall of CT. The region between the first and the second *walls* of CT appear as a *lobe* of tumor cells. The process then repeats, leading to successive lobes. They used CT-concentration dependent diffusion coefficient for the TCs.

The model used by Perumpanani *et al.*[22] is extended in this study in two specific ways. First, the tumor cell generation term is generalized to simulate more complex growth than is possible by the growth model used by them. Second, the simulations are carried out in one-dimensional Cartesian, as well as cylindrical and spherical geometries. In certain cases, as is shown below, the difference between the results for different geometries can be quite significant.

MODEL

The partial differential equations governing the balance of the tumor cells $m(r,t)$, and connective tissue $c(r,t)$ are[22]

$$\frac{\partial m(r,t)}{\partial t} = g(m,c) + \left[\frac{\partial J_m(r,t)}{\partial r} + \frac{n}{r} J_m(r,t)\right] \tag{1}$$

$$\frac{\partial c(r,t)}{\partial t} = k\left|\frac{\partial [c(r,t) J_m(r,t)]}{\partial r} + \frac{n}{r} c(r,t) J_m(r,t)\right| \tag{2}$$

where $g(m,c)$ is the generation term, J_m is the tumor cell flux, and n is *0, 1* or *2* for Cartesian, cylindrical and spherical geometries, respectively. [The definition of J_m used here is slightly different from that in Ref. 22.] Note that the connective tissue does not diffuse—it is only convected by the diffusing tumor cells. The connective tissue flux is proportional to the connective tissue concentration $c(r,t)$ and the tumor cell flux J_m. Parameter k is a key parameter in the model that represents the ability of the diffusing tumor cells to convect the connective tissue. The source term $g(m,c)$ is of the form

$$g(m,c) = \gamma(c)\, m(1-m)^b \tag{3}$$

where γ models the dependence of tumor cell growth on the local connective tissue concentration. For smaller concentrations of $c(r,t)$, $\gamma(c)$ is expected to be one; however, for regions with large concentrations of $c(x,t)$ such as at the wall, $\gamma(c)$ can be less than one signifying the dense acellular region within the capsule itself which provides limited support, if at all. In this study we have analyzed both $\gamma(c) = 1$, and when $\gamma(c)$ varies as

$$\gamma(c) = \frac{1 - \tanh[a_1(c - a_2)]}{2} \tag{4}$$

where a_1 and a_2 are constants. In equation (3), b is a constant, and values of $b > 1$ are necessary to simulate an asymmetric growth: a faster growth rate when $m(r,t)$ is small, and a slower growth rate as the concentration approaches its saturation value of one. With $b = \gamma(c) = 1$, this generation term reduces to the standard quadratic form.[18,22]

The tumor cell flux is assumed to be of the form[22]

$$J_m(r,t) = \theta(c)\, m(r,t)^p \frac{\partial m(r,t)}{\partial r} \tag{5}$$

where $\theta(c)$ is the CT-concentration dependent diffusion coefficient for the tumor cells. The generalized nonlinear form for the flux is necessary to simulate certain biological dispersions.[18,22] [$p = 0$ represents Ficksian diffusion.] A value greater than one for p represents a diffusion process that not only is proportional to the gradient, but also to the magnitude of the concentration itself.[18] Perumpanani *et al.*[22] used $p = 0$ and 1 in their study. Equation (1) with $p = 0$, a quadratic source term ($\gamma(c) = b = 1$) and $\theta(c) = 1$, reduces to the well known Fisher equation which results in a solution that evolves into a traveling wave with a smooth front.[15] On the other hand, for $p = 1$, the wave has a sharp front.[18,19,22] In this case, the concentration decreases to zero at say, $r_w(t)$ ($< \infty$), and the solution is zero for $r > r_w(t)$. Exact analytical solutions for special cases of the nonlinear diffusion case with simple quadratic growth term are available.[16] Substituting the expressions for J_m and $g(m,c)$ in Eqs. (1) and (2), we get

$$\frac{\partial m(r,t)}{\partial t} = \gamma(c)\, m(r,t)(1 - m(r,t))^b + \frac{\partial}{\partial r}\left[\theta(c)\, m^p \frac{\partial m}{\partial r}\right] + \frac{n}{r}\theta(c)\, m^p \frac{\partial m}{\partial r} \tag{6}$$

$$\frac{\partial c(r,t)}{\partial t} = k\left[\frac{\partial}{\partial r}\left[c(r,t)\,\theta(c)\, m^p \frac{\partial m}{\partial r}\right] + \frac{n}{r} c(r,t)\,\theta(c)\, m^p \frac{\partial m}{\partial r}\right]. \tag{7}$$

A simple explicit finite difference scheme with upwinding is used to solve the above set of PDEs. We have used $\Delta x = 0.05$ and $\Delta t = 0.001$. See Ref. 22 for details.

NUMERICAL RESULTS

Calculations were performed in $0 \le r \le \infty$ with symmetry boundary conditions at $r = 0$ for both $m(r,t)$ and $c(r,t)$ as

$$\frac{\partial m(r=0,t)}{\partial r} = 0; \qquad \frac{\partial c(r=0,t)}{\partial r} = 0 . \tag{8}$$

As r approaches infinity, both $m(r,t)$ and $c(r,t)$ should approach their initial values at infinity. In numerical calculations, we make sure that the spatial domain is large enough that the concentrations at the end of the simulations in a region at the right edge ($r = r_{max}$) of the spatial domain do not change from their initial values.

The tumor cell concentration is initially zero everywhere except in a small region close to the origin, $0 \le r \le r_m$. The concentration in this region at $t = 0$ drops linearly from m_0 at the first grid point with $r > 0$, to zero at r_m. There are two different types of initial conditions used for $c(r,t=0)$. First is the same as that used by Perumpanani *et al.*[22] In this initial condition, which will be called IC-1, the connective tissue concentration is c_0 for $r_c \le r \le \infty$, and zero for $0 \le r \le r_c$. In the second type of initial condition (IC-2), $c(r,t=0) = c_0$ for $0 \le r \le \infty$. In all calculations reported here, $r_m = 2.5$, $r_c = 5.0$, and $\theta(c) = 1$. Note that when $\theta(c) = \gamma(c) = 1$, Eq. (6) is independent of Eq. (7).

Results for two different values of k for the Cartesian, cylindrical and spherical geometries with $b = 1$, $\gamma(c) = 1$, and initial conditions of type IC-1 are shown in Figs. 1 and 2. For $k = 3.5$, in Cartesian geometry, as expected, the moving front of the TC concentration $m(r,t)$ has a sharp edge, and moves forward with the characteristic velocity of $1/\sqrt{2}$ (Fig. 1a). The CT concentration $c(r,t)$ quickly evolves into a high density region (the wall) that is convected outward by the moving front of the TC concentration. For $k = 4.1$, the magnitude of the $c(r,t)$ spike does not saturate, but rather continues to increase as the wall is convected toward the right[22] (Fig. 2a). Simulations for the cylindrical and spherical geometries show similar trends (Figures 1b, 1c and 2b, 2c), but the magnitude of the peak of the $c(r,t)$ wall is smaller when compared to the peak in the Cartesian coordinate system, and takes longer in time to evolve. Note the different scales used for the vertical axes in these figures. Because there is only one-way coupling between Eqs. (6) and (7), once $m(r,t)$ grows to its saturation value of 1, all evolution ceases in that region of space. With $b = 1$, this happens very quickly near the origin. Coupled with the high convection strength (large k) and the particular type of initial condition (IC-1), the region near the symmetry plane (or origin) is quickly depleted of $c(r,t)$.

There is physical motivation to modify the generation term to slow down the generation of tumor cells as m approaches its saturation value. The generation of $m(r,t)$ is parameterized by $\gamma(c)$ and the parameter b. With $\gamma(c) = b = 1$, the normalized generation with $m(r,t) = 0.9$ is the same as that with $m(r,t) = 0.1$. With high population pressure, it is quite likely that in reality, the generation with $m(r,t) = 0.9$ is actually less than that with $m(r,t) = 0.1$. This is accomplished by a b that is greater than 1. The effect of the paramater b is shown in Fig. 3 for $b = 2$. Here $\gamma(c) = 1$, hence the growth is still independent of the local CT concentration, $c(r,t)$. Slower growth of the TC is evident. Moreover, as a result, the peak of the CT concentration is significantly lower than that for the corresponding $b = 1$ case. In Cartesian geometry, the peak, even for $k = 4.1$, saturates at a maximum concentration of CT that is less than one, whereas previously the

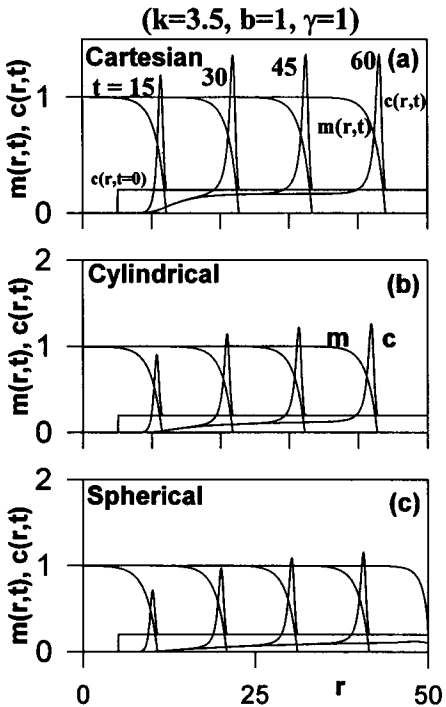

Figure 1. Tumor cell and connective tissue distribution starting from IC-1. c(r,t=0) is also shown in the figures. a) Cartesian, b) cylindrical, c) spherical.

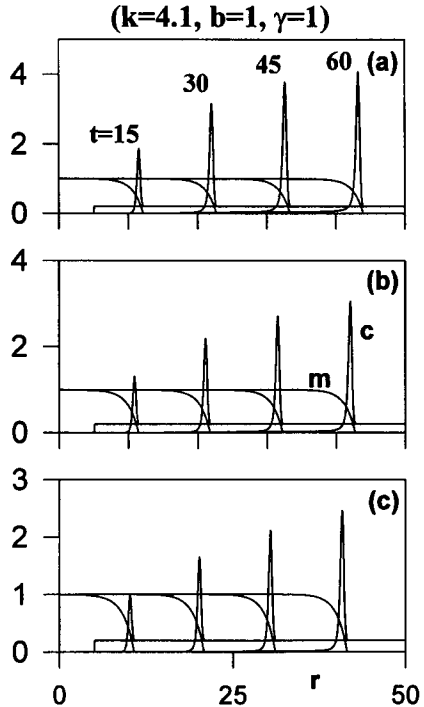

Figure 2. Effect of a higher value value of k on the evolution. All parameters values are the same as in Figure 1 except $k = 4.1$.

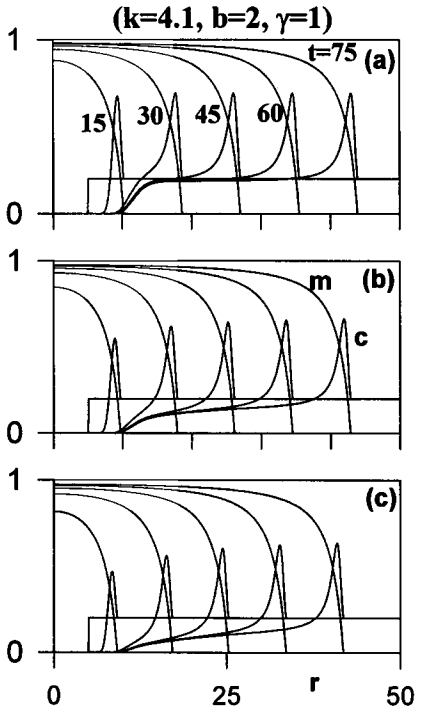

Figure 3. Effect of an asymmetric population pressure on growth. All parameter values are the same as in Figure 2 except $b = 2$.

peak magnitude for the $b = 1$ case was greater than 4 and growing (Fig. 2a.) Hence, $b > 1$ increases the critical value of the convection strength k at which the bifurcation from a constant amplitude wall of CT to a peak with a growing amplitude occurs.[22]

The effect of different initial conditions (IC-2, rather than IC-1) on the evolution of the TC and CT concentration is studied in Fig. 4 where all the parameters (k, b, and θ) are the same as in Fig. 3. Comparison of Figs. 3 (a-c) with Figs. 4 (a-c) shows that the evolution from this set of initial conditions (IC-2) is significantly different from that obtained using IC-1. In the absence of any physical reason for using initial condition of type 1 (originally used in Ref. 22), all subsequent calculations were carried out using IC-2.

The effect of the generation term's dependence on the CT concentration is studied next. With $a_1 = 10$ and $a_2 = 1$ in Eq. (4), the generation as a function of $c(r,t)$ rapidly decreases from one to zero in a thin interval around $c(r,t) = 1$. This would take into account the population pressure on generation due to high local concentration of the CT, such as at the wall. Results are presented for $k = 5$, and $b = 1$ and 2 in Figures 5 through 8. In Figure 5, that shows the results for $b = 1$ case, the high value of k coupled with a small value for b, leads to a traveling spike of $c(r,t)$ with growing amplitude in all three coordinate systems. As b is changed to 2, the evolution of CT changes significantly. Figure 6 shows the evolution in Cartesian geometry at $t = 40$, 80 and 200. The spike in $c(r,t)$ ($t = 40$, panel 6a), grows and travels forward. Simultaneously, the lack of generation (due to $\gamma(c)$) at the spike leads to the development of another smaller spike slightly ahead of the major one. Due to the sharp gradient in $m(r,t)$ at the wavefront (the tumor edge), the convection rates of the two spikes (and their growth rates) are significantly different. Consequently, they grow apart. The first one almost stops at $r \approx 22$ as the TC concentration at that location is fully developed to its saturation value, and no longer provides any convection to the CT (panel 6b). The smaller spike at the front of the TC wave then repeats the same process again spawning more regions of dense CT. In Cartesian geometry, the result—shown in panel 6c at $t = 200$—is a sequence of thin regions (walls) of dense CT separated by tumor cells. Though the resulting structure resembles a nodular tumor, unfortunately—unlike in many benign nodular tumors—in Cartesian coordinates, the innermost spike is the most dense, and the density at the first three spikes decreases with increasing distance of those spikes from the origin.

The evolution in the cylindrical geometry ($n = 1$) is somewhat different. The physical process is the same as in the Cartesian geometry, but the geometry effect leads to unevenly spaced spikes with mixed amplitudes. Figure 7 shows the m and c distribution as a function of r in cylindrical geometry at $t = 200$. In spherical geometry ($n = 2$), Fig. 8, the innermost spike has the smallest magnitude, mimicking the structure in a benign nodular tumor. Moreover, the results suggest that the innermost lobe of tumorous cells is expected to be bigger than those near the capsule.

DISCUSSION

The current model is capable of simulating the evolution of the tumor cells and connective tissue resulting in either a single homogeneous region of tumor cells *encircled* by a thin region of highly concentrated connective tissue, or several *lobes* of tumor cells separated by walls of connective tissue of varying concentrations. The CT concentration at the walls depends upon the coordinate system in which the simulation is carried out. In Cartesian coordinates, for parameter values studied, the concentration of the innermost

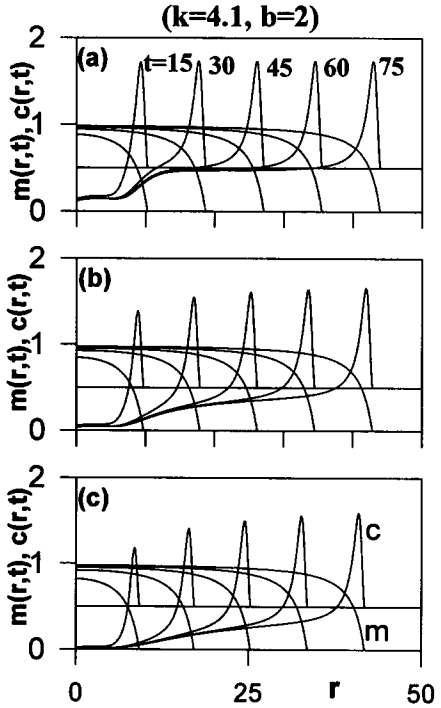

Figure 4. Effect of a different initial condition (IC-2). All parameter values are the same as in Figure 3.

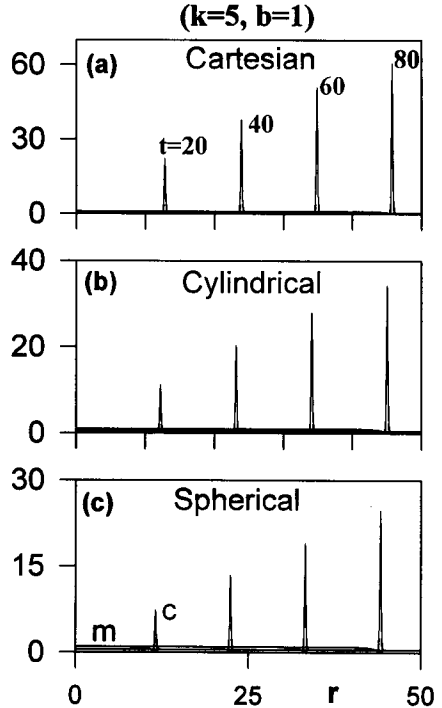

Figure 5. Effect of connective tissue population on the growth of the tumor cell via $\gamma(c)$ given by Eq. (4). Here $a_1 = 10$, $a_2 = 1$, $k = 5$, $b = 1$.

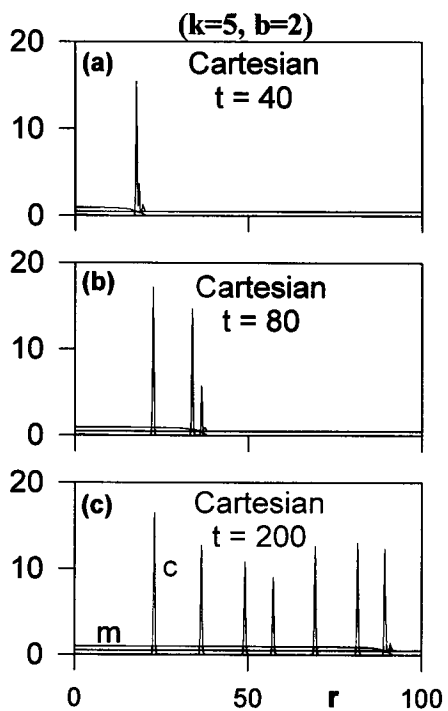

Figure 6. Combined effect of the parameter b and $\gamma(c)$. Here $b = 2$ and $\gamma(c)$ and all other parameters are as in Figure 5. a) t = 40, b) t = 80, c) t = 200.

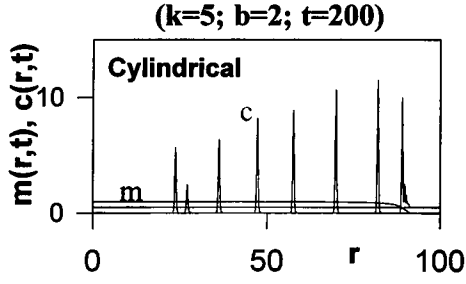

Figure 7. Tumor cell and connective tissue concentration in cylindrical geometry at $t = 200$. All parameters are the same as in Figure 6.

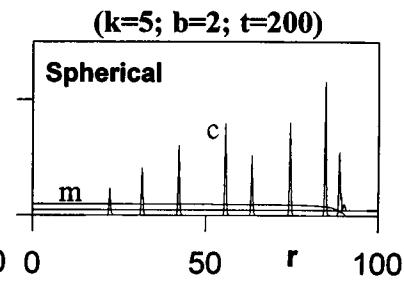

Figure 8. Tumor cell and connective tissue concentration in spherical geometry at $t = 200$. All parameters are the same as in Figure 6.

wall is found to be the highest. On the other hand, in spherical coordinates, the magnitude of the CT concentration peaks near the center is much smaller than those near the edge. Moreover, the results obtained using spherical coordinates also suggest that in the case of nodular tumors, the innermost lobes are likely to be bigger than those near the capsule walls.

In our model, the pressure on growth due to local population of TC was taken into account by the parameter b. A value of $b > 1$ leads to the asymmetry described before, and slows the generation in regions with high concentration of tumor cells. This accounts for the physical fact that *per individual cell*, less of the support services are available for these cells to multiply. The effect of high concentration of connective tissue on tumor cell generation was included through the parameter $\gamma(c)$. When $\gamma \neq 1$, its dependence on c is such that the tumor cell generation is stopped only where CT concentration is very large—i.e. essentially only within the narrow regions of the CT walls. The combination of choice for b and γ causes the TC multiplication to occur only in a narrow region near the capsule wall within the body of the tumor where both m and c are small.

The model used here does not take into account several physiological details. For example, it is well known that the connective tissue stroma itself can regulate the access of inflammatory cells,[3] and that tumor cells depend on nearby supportive stroma in a way that being 1 to 2 mm away from a blood vessel may cause cell death. Future models and simulations should also take into account the histological evidence that suggests that low concentrations of cross-linked fibrin (e.g., 1 mg per milliliter) is more amenable to macrophage migration than higher fibrin concentrations (e.g., 3 mg per milliliter), which are virtually impenetrable.[3] Moreover, the model has been solved here only in *one-dimensional* Cartesian, cylindrical and spherical coordinates. Simulations in multi-dimensions should be carried out to better understand tumor growth and encapsulation.

REFERENCES

1. COTRAN, R. S., V. KUMAR & S. L. ROBBINS. 1994. Pathologic basis of disease, 5th ed., WB Saunders. Phladelphia, PA.
2. SLEEMAN, B. D. 1996. Solid tumor growth: A case study in mathematical biology. Nonlinear mathematics and its applications. Cambridge University Press. Cambridge, UK.
3. DVORAK, H.F. 1986. Tumors: Wounds that do not heal—Similarities between tumor stroma generation and wound healing. N. Engl. J. Med. **315**: 1650-1659.
4. BARR, L.C., R.L. CARTER & A.J.S. DAVIES. 1988. Encapsulation of tumors as a modified wound healing response. Lancet 135-137 , July 16, 1988.
5. EWING, J. 1940. Neoplastic diseases, 4th ed., WB Saunders. Philadelphia, PA.
6. ENNEKING, W. F. 1983. Musculoskeletal tumor surgery. pp. 3-68. Churchill Livingstone. Edinburgh, UK.
7. CAMERON, E. 1982. Vitamin C and cancer: An overview. Int. J. Vitam. Nutr. Res. **23**: 115-127.
8. BALDWIN, R. W. & M. V. PIMM. 1980. Human tumour xenografts in athymic nude mice: non-specific host rejection responses. *In* Sparrow S, ed., Immunodeficient animals for cancer research. Medical Research Council. London, UK.
9. BARR, L. C. 1980. The encapsulation of tumours [MS Thesis]. University of Manchester. Manchester, UK.
10. SHERRATT, J. A. & J. D. MURRAY. 1990. Models of epidermal wound healing. Proc. R. Soc. Lond., B **241**: 29-36.
11. ADAM, J. A. 1986. A simplified mathematical model of tumor growth. Math. Biosci. **81**: 229-244.
12. ADAM, J. A. 1987. A mathematical model of tumor growth II: Effects of geometry and spatial nonuniformity on stability. Math. Biosci. **86**: 183-211.
13. ADAM, J. A. 1987. A mathematical model of tumor growth III: Comparison with experiment. Math. Biosci. **86**: 213-217.
14. VAIDYA, V. G. & F. J. ALEXANDRO, JR. 1982. Evaluation of some mathematical models for tumor growth. Int. J. Bio-Medical Computing **13**: 19-35.
15. SACHDEV, P. L. 1987. Nonlinear diffusive waves. Cambridge University Press. Cambridge, UK.
16. NEWMAN, W.I. 1980. Some exact solutions to a non-linear diffusion problem in population genetics and combustion. J. Theor. Biol. **85**: 325-334.
17. BRITTON, N. F. 1986. Reaction-diffusion equations and their applications to biology. Academic Press.
18. MURRAY, J. D. 1989. Mathematical biology. Springer-Verlag.
19. SHERRAT, J. A. & B. P. MERCHANT. 1996. Nonsharp traveling wave fronts in the Fisher equation with degenerate nonlinear diffusion. Appl. Math. Lett. **9**: 33-38.
20. RIZWAN-UDDIN. 1997. An improved coarse-mesh nodal integral method for partial differential equations. Num. Methods for Partial Diff. Equations **12**: 113-145.
21. SHERRAT, J. A. & M. A. NOWAK. 1992. Oncogenes, anti-oncogenes and the immune response to cancer: A mathematical model. Proc. R. Soc. Lond., B **248**: 261-271.
22. Perumpanani, A. J., J. A. Sherratt & J. Norbury. 1996. Mathematical modeling of capsule formation and multi nodularity in benign tumor growth. Warwick Preprint: 51/1996, University of Warwick. Coventry, UK.